JOURNAL OF MATERIALS SCIENCE 29 (1994) 4268–4272

Microstructural characteristics and gas content of rapidly solidified powders

J. S. DUNNING, R. C. DOAN
US Bureau of Mines, Albany Research Center, Albany, OR, USA

The gas content and microstructural characteristics of rapidly solidified powders manufactured by different techniques were studied by Bureau of Mines researchers. Powders were screened and classified into size fractions. Powder characteristics including gas content and porosity were measured and related to powder particle size. Three different atomizing gases, argon, helium, and nitrogen were used in manufacturing the powders. In one series of experiments one gas was used to atomize the melt while a different gas was used in the melting and powder collection chambers. The gas content of the powders was shown to consist of three separate components: (1) solid solution, (2) physical entrapment associated with macroporosity, and (3) surface reaction such as surface oxide. The various components of gas content could be identified by the shape of the curve plotting gas content versus particle size. The identification of the presence of entrained gas as porosity from these curves is important because after consolidation, high-pressure bubbles of inert gas can result. This porosity can cause problems during subsequent heating or joining operations, seriously degrading mechanical properties. Analysis of gas content versus particle size represents a sensitive, technique to detect the presence of porosity.

1. Introduction

The commercial application of rapidly solidified iron-base alloys has been limited largely to the aerospace industry. A number of atomizing techniques, notably inert gas atomization (IGA) and centrifugal atomization (CA) are used for commercial production of powders. Rapidly solidified powders are rather arbitrarily defined by a cooling rate of greater than $10^2\,^{\circ}C\,s^{-1}$ [1–3]. Powders are typically atomized and/or cooled convectively by large quantities of gas (usually argon, helium, or nitrogen). This study was undertaken to determine how powder particles interact with these gases as well as with residual trace gases, such as oxygen, in the atomizing chamber or in the atomizing gas. Molten droplets, with their large combined surface area are effective getters for any residual trace oxygen.

The interaction of both inert and reactive gases with the metal particles during atomization can have a significant effect both on the powders and the subsequently consolidated product. Surface oxide films, inert gas entrapped as porosity and solid solution additions can all significantly affect the product following consolidation of rapidly solidified powders.

2. Experimental procedure

Powders from a variety of sources were characterized. All the powders studied were made by inert gas atomization (IGA) or centrifugal atomization (CA). The study included commercial powders and powders from research atomizers. The gases in the powder atomizing process were used to break up the melt stream (atomizing gas in the IGA process), to cool convectively the powder particles (chamber gas), to shield the melt during melting or were present as trace impurities.

Analysis for noble gas (helium, argon) concentrations was performed by fusion mass spectrometry [4]. Nitrogen and oxygen analyses were performed by fusion analysis. The general morphology of the sized powders and porosity determinations were carried out using standard metallographic preparation and scanning electron microscope studies.

3. Results

3.1. Powder morphology, porosity, and gas content

A group of type 304 stainless steel powders manufactured by either inert gas atomization (IGA) or centrifugal atomization (CA) was characterized. In inert gas atomization, a high-velocity gas stream breaks up a molten metal stream into fine particles. The particles are cooled in inert gas during solidification. In centrifugal atomization a molten stream of metal impinges on a rotating cup or dish and is centrifugally atomized into fine droplets which are subsequently quenched with high-pressure inert gas jets. Seven powders were analysed for gas content, porosity, geometry and size distribution. A summary of information on all atomizing runs is shown in Tables I and II. In the first series of experiments (Table I) the same atomizing gas is used in the high-pressure jet nozzle that atomizes

0022–2461

TABLE I Characterization of some 304 SS powders atomized by different techniques and from a variety of manufacturing sources

Powder ID	Atomization method[a]	Atomization or quench gas	Chamber backfill gas	Helium content (at p.p.m.)	Argon content (at p.p.m.)	Nitrogen content (at p.p.m.)	Oxygen content (at p.p.m.)	Porosity	Mean particle size (μm)
A	CA	He	He	8	< 0.1	ND	600	Low	80
B	IGA	Ar	Ar	ND[b]	2.5	250	700	High	70
C	IGA	He	He	1.5	< 0.1	ND	1100	None	60
D	IGA	Ar	Ar	ND	4.6	1200	900	High	50
E	IGA	N	N	ND	< 0.1	5800	850	None	50

[a] CA, centrifugal atomization; IGA, inert gas atomization.
[b] ND, not determined.

TABLE II Characterization of some 304 SS powders atomized by inert gas atomization using the same atomizing unit but different atomizing and chamber gas combinations

Powder ID	Atomizing gas	Chamber backfill gas	Argon content (at p.p.m.)	Nitrogen content (at p.p.m.)	Oxygen content	Porosity
D	Ar	Ar	4.6	1200	900	High
E	N	N	< 0.1	5800	850	None
F	Ar	N	2.6	6150	850	High
G	N	Ar	< 0.1	3000	1200	Trace

the melt stream (or in the case of CA the high-flow gas that quenches atomized particulate) and in the quenching chamber. All powder particles were spherical with some small satellites. Powder B was the most irregular powder with the greatest number of satellites. A micrograph of a grab sample of powder B together with micrographs of powders D and E are shown in Fig. 1. A higher magnification micrograph of powder E is shown in Fig. 2. Mean particle sizes are presented in Table I. Powders C, D, and E had the smallest mean particle size reflecting the use of research atomizers rather than commercial production atomizers. It is feasible to operate research atomizers at parameters closer to nozzle freeze-up. Powders B, D, and E had the widest size distribution in the range − 20 to + 150 μm. The powders were broken down to six size fractions. The exact size fractions used varied with the size distribution of the particular powder. Samples from the various size fractions for each powder were mounted, sectioned and polished to study porosity. High porosity was observed in the two

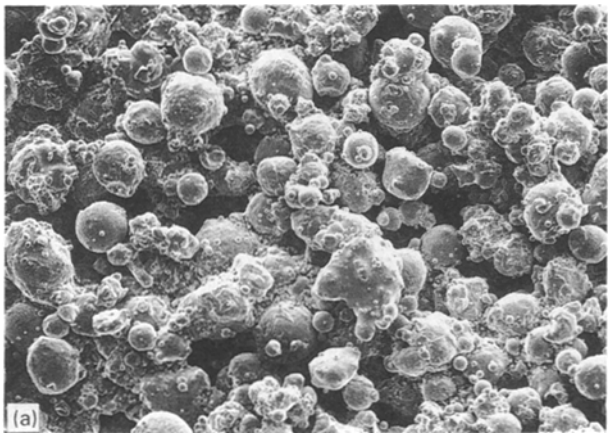

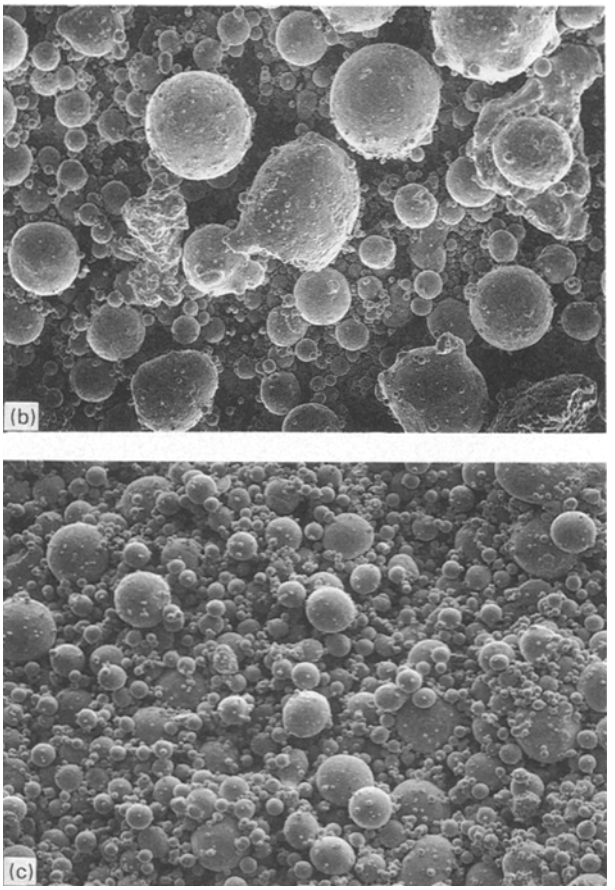

Figure 1 Grab samples of (a) powder B, (b) powder D, and (c) powder E. × 200.

argon-atomized powders B and D. Trace porosity was observed in powder A. Micrographs of a representative sample of the 75–100 μm fraction of powder A and a micrograph of a metallographic cross-section of

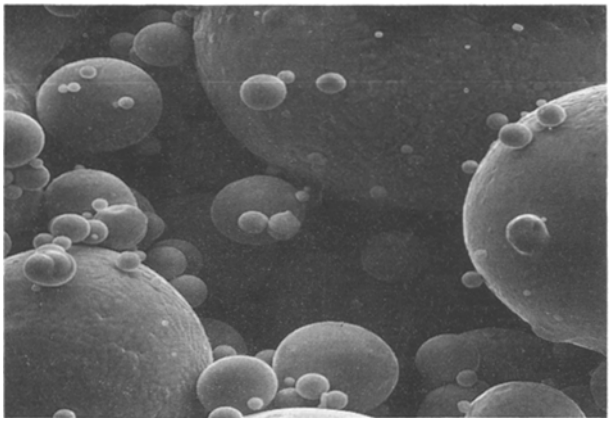

Figure 2 Grab sample of powder E. × 1500.

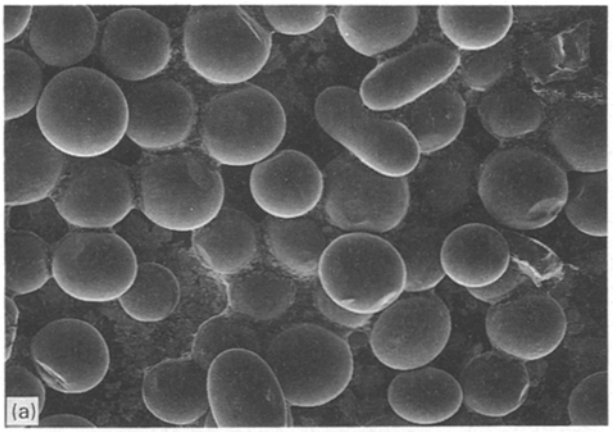

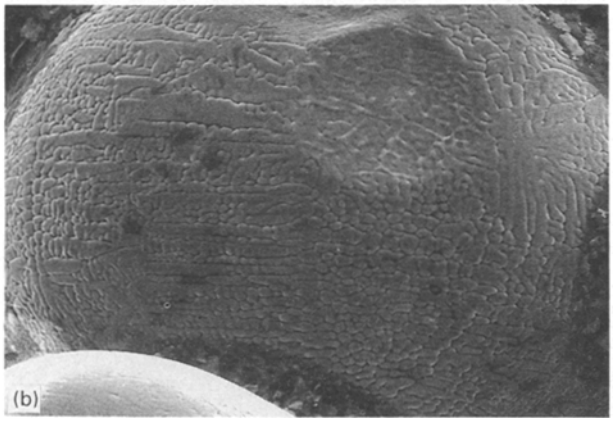

Figure 3 Powder A, size fraction 75–100 μm. (a) × 200, (b) × 1500.

the same size fraction are shown in Figs 3 and 4, respectively. These micrographs can be compared with similar micrographs of the two high-porosity powders, powder D shown in Fig. 5a, b and powder B shown in Fig. 5c, d. Even in these latter two powders it can be clearly seen that the porosity is different. In powder D the pore surface is smooth and the pores are round, characteristic of gas bubbles. In powder B the bubbles are non-uniform and distributed throughout the powder particles, more reminiscent of interdendritic shrinkage pores. The number of particles with porosity increases with particle size. By mounting samples of powders D and B and step polishing

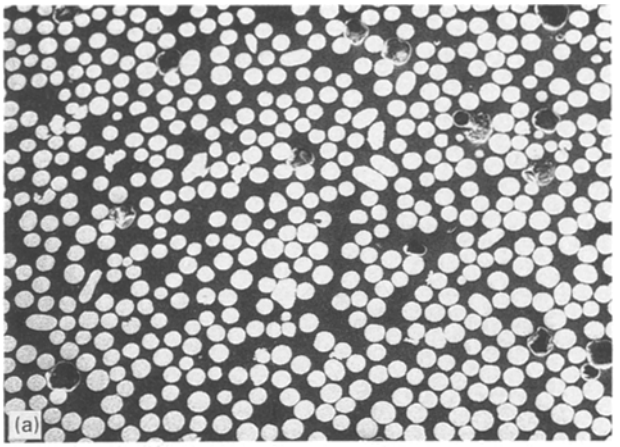

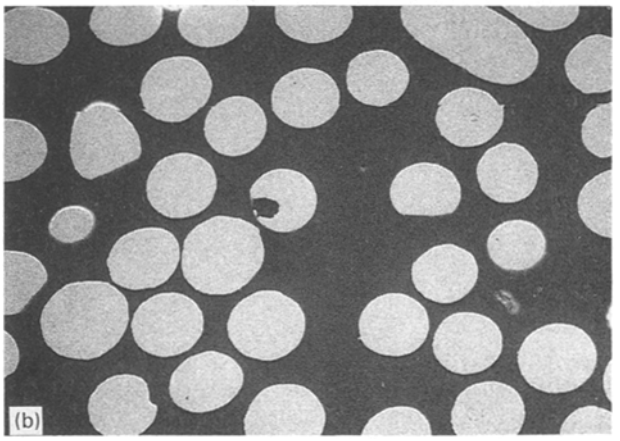

Figure 4 Powder A, size fraction 75–100 μm, polished cross-section. (a) × 50, (b) × 200.

through several layers of powder, it was determined that (1) there is only minimal porosity below a particle size of 45 μm, and (2) for size fractions with a mean particle size of 45, 90, and 125 μm the percentage of particles with at least one pore was 53%, 65%, and 93%, respectively, for powder B and 40%, 84%, and 67% for powder D.

Evidence for a relationship between porosity and gas content is shown in Fig. 6 where the atomizing gas content (helium, argon) in atomic parts per million (at p.p.m.) is plotted as a function of particle size for powders D, B, and C. The atomizing gas content tends to increase with particle size, as does porosity. The gas content at a particle size of 20 μm ($\sim$ 1 at p.p.m.) is assumed to be related to the solid solubility achieved during rapid solidification; the increased gas levels are interpreted as being gas entrapped within pores and not in solid solution. Even for powder C, where little porosity was detected, the same relationship holds.

The variation of oxygen content of powders with particle size is shown in Fig. 7. Powders A, B, and C all exhibited the same type of variation of oxygen content with particle size plotted for powder B in Fig. 7. Oxygen decreases with increasing powder size consistent with a $1/r^2$ relationship (where r is the particle radius) indicative of oxygen being present as a surface oxide. An interesting anomaly was observed for the oxygen content variation with particle size for powder D. While the curve for powder D shows the same variation with particle size as powder B below a

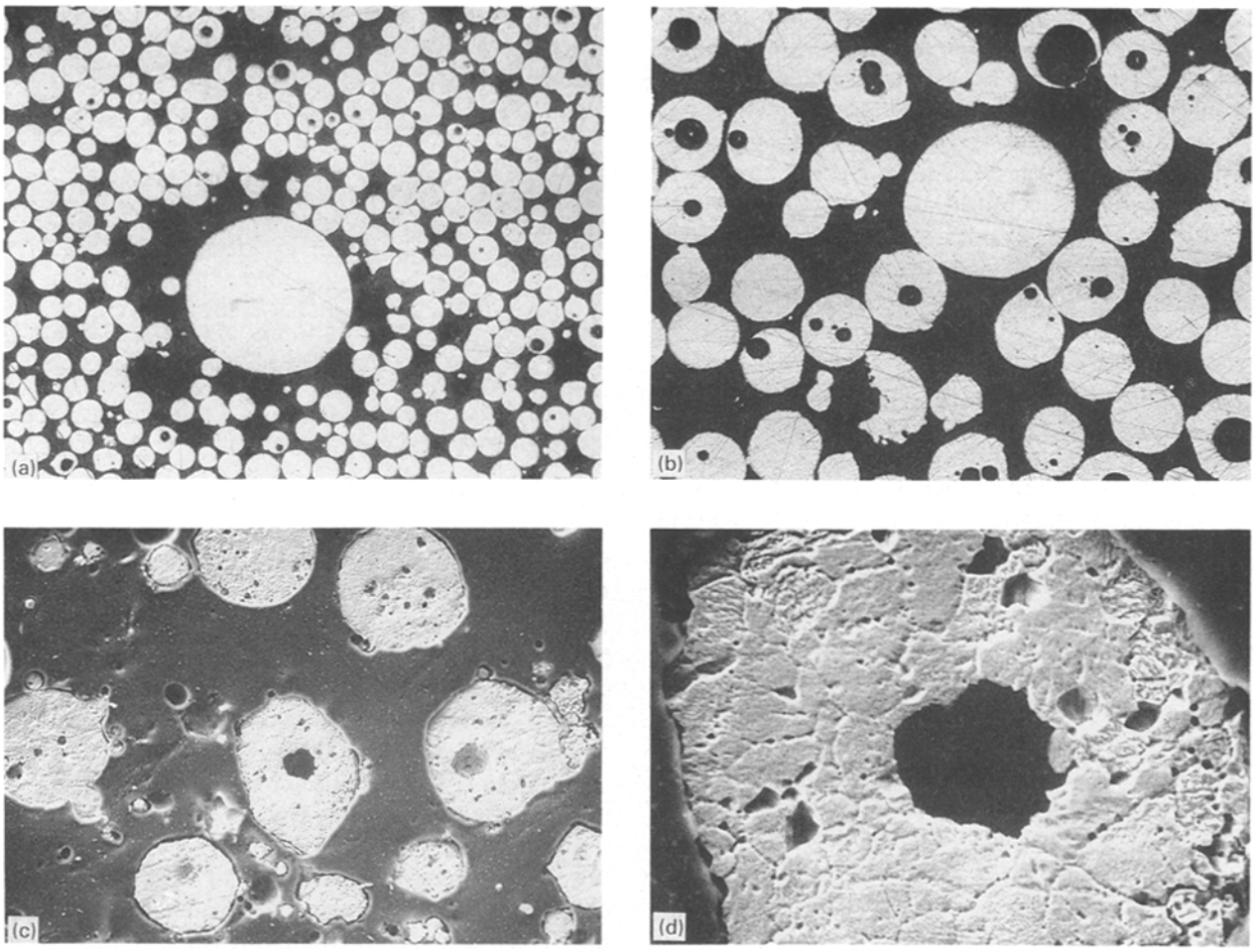

Figure 5 (a, b) Powder D; (a) size fraction 38–53 μm, × 100. (b) size fraction 104–147 μm, × 100. (c, d) Powder B grab sample, (c) × 200, (d) × 1000.

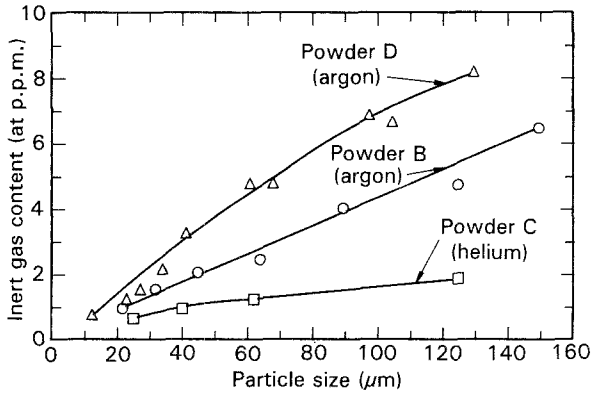

Figure 6 Inert gas (atomizing gas) content of powders as a function of particle size.

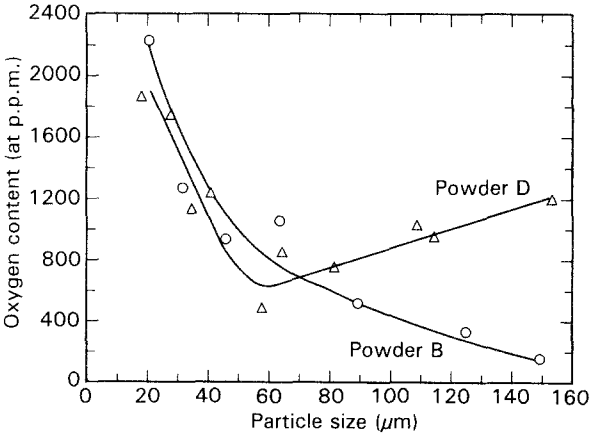

Figure 7 Variation of oxygen content of powder particles with powder particle size.

particle size of approximately 50 μm, above this particle size the oxygen content of powder D increases significantly with powder particle size. The 50 μm particle size is the particle size at which significant porosity begins to be observed in powder D. The shape of the oxygen content versus particle size curve for powder D was characteristic of the oxygen curves for all powders produced in one research atomizer (used for powders D, E, F, and G). It is evident that increasing oxygen content with particle size above a particle size of 50 μm is associated with increasing porosity with particle size in these same powders. This could be associated with insufficient deoxidation of the melt or oxygen contamination of the argon atomizing gas used in this atomizer as compared with the commercially produced argon atomized powder (powder B). This explanation will be discussed further in a more detailed breakdown of these data plots in the next section.

To study the source of porosity, entrapment, and solution of gases such as nitrogen, argon, and oxygen,

a series of experiments was run on a research atomizer where the atomizing nozzle gas and cooling chamber gas could be varied independently. For these experiments the melt shield gas and the chamber cooling gas was the same while the atomizing nozzle gas was varied. Thus the source of inert gas entrapment as porosity could be identified as porosity from entrapment of the nozzle gas or chamber gas during formation and cooling of the metal droplet. The solubility of soluble gases could also be tied to solubility occurring in the melt or in the droplet during non-equilibrium solidification.

The matrix of gases used and the resulting gas contents and porosity are shown in Table II. It is apparent that high porosity is associated with the use of argon as an atomizing gas for type 304 stainless steel and that in turn leads to high argon contents in the resulting powder. High nitrogen contents, on the other hand, are associated with nitrogen used as a backfill gas in the atomizing chamber and as a shield gas above the melt. The high solubility of nitrogen in the melt (as compared with argon and helium) leads to higher concentrations of nitrogen in the resulting powder.

The nitrogen concentration of the powders showed no variation with particle size. A straight line plot was recorded for all nitrogen containing powders over the 0–160 μm size range.

4. Discussion and conclusions

A study of the gas contents of the inert and reactive gases used in this study and the variation of the gas content with particle size indicates there are three components contributing to total gas content.

(a) Entrained noble gases associated with porosity: an increase of gas content with particle size of inert gases such as argon and helium is associated with porosity in the powder particles. The solubility of these gases in metals is extremely low (1 at p.p.m. or less). A plot of inert gas content versus particle size for powders B, C, and D is plotted in Fig. 6. The inert gas content at very low particle sizes where zero porosity is observed is of the order of 1 at p.p.m. or less. No significant porosity was detected in powder C with inert gas content of less than 2 at p.p.m. Porosity was observed in the particle size fractions above 40 μm for powders B and D where inert gas content climbed above 2 at p.p.m. to the 6–8 at p.p.m. range. It is likely that inert gases are mechanically entrained during the formation of molten droplets [5].

(b) Solid solution of gases: the solution of gases such as nitrogen and oxygen that are soluble in significant amounts in molten iron are usually determined by melt conditions and do not vary with the size of the powder particle.

(c) Surface reaction with reactive gases: surface reactions during solidification and cooling of the powder particle (such as surface oxidation) can change the gas content of a powder particle. The increase in gas content of this component will vary with the relative surface area to volume of the particle and will decrease with the size of the particle in a $1/r^2$ relationship.

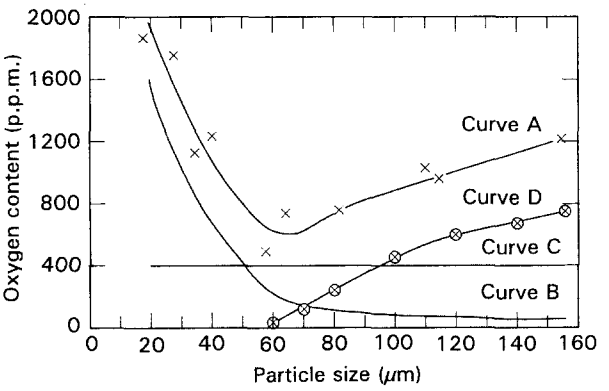

Figure 8 Master curve A (a plot of oxygen content versus particle size) is broken down into three component curves B, C and D.

An analysis of the breakdown of the various components of gas content and the prediction of an increase in gas content associated with macroporosity can be demonstrated by replotting the powder D oxygen curve from Fig. 7. This curve of oxygen content variation with particle size is replotted as curve A in Fig. 8. By extrapolating curve A back to a particle size of 10 μm then plotting an oxygen content from this point directly proportional to $1/r^2$, curve B is obtained to represent the surface oxide component of the oxygen content. By comparing curve B with curve A below a particle size of 50 μm (where no significant porosity was observed), a bulk oxygen content of approximately 400 p.p.m. was estimated. This component does not change with particle size and can be plotted as curve C. By subtracting curves B and C from curve A, curve D is obtained. This is oxygen content associated with physical entrapment of oxygen during the formation of macroporosity. The shape of the combined oxygen content curve as it varies with particle size can thus be taken as a positive indication of porosity in powder particles above the 50 μm size range. This porosity will typically be associated with the physical entrapment of the inert gas used to atomize the powder.

References

1. M. COHEN, B. H. KEAR and R. MEHRABIAN, in "Proceedings of the Second International Conference on Rapid Solidification Processing: Principles and Technologies II", edited by R. Mehrabian, B. H. Kear and M. Cohen (Claitors, Baton Rouge, LA, 1980) pp. 1–23.
2. J. E. FLINN, in "Rapid Solidification Technology for Reduced Consumption of Strategic Materials" (Noyles, Park Ridge, NJ, 1985) p. 18.
3. R. MEHRABIAN, *Int. Metall. Rev.* **27** (1982) 184.
4. G. R. SMOLIK and J. E. DELMORE, *Mater. Sci. Eng.* **A124** (1990) 15.
5. J. E. FLINN and G. R. SMOLIK, *ibid.* **A124** (1990) 39.

Received 30 March 1993
and accepted 28 February 1994